Photodissociation of the alkali iodides at 347.1 nm: Experimental angular distributions and dynamic model for their interpretation

William R. Anderson, Bradley M. Wilson, Raleigh C. Ormerod, and Timothy L. Rose

Citation: The Journal of Chemical Physics **74**, 3295 (1981); doi: 10.1063/1.441536
View online: http://dx.doi.org/10.1063/1.441536
View Table of Contents: http://scitation.aip.org/content/aip/journal/jcp/74/6?ver=pdfcov
Published by the AIP Publishing

Photodissociation of the alkali iodides at 347.1 nm: Experimental angular distributions and dynamic model for their interpretation

William R. Anderson,[a,b] Bradley M. Wilson, Raleigh C. Ormerod,[c] and Timothy L. Rose[a,d]

Department of Chemistry, Texas A&M University, College Station, Texas 77843
(Received 8 September 1980; accepted 25 November 1980)

The angular distributions of the alkali photofragment resulting from photodissociation of a molecular beam of NaI, KI, CsI, or RbI by a pulsed, linearly polarized laser beam at 347.1 nm have been measured. At the wavelength used, only production of ground state atoms is energetically feasible. The angular distributions indicate a trend in the perpendicular:parallel transition ratio from about 4:1 for NaI to about 2:1 for RbI and CsI. This interpretation assumes Hund's case (c) coupling and excited states of pure perpendicular or parallel symmetry. A new model was developed to calculate the laboratory distribution from any center of mass distribution, including those resulting from multiphoton or saturated transitions. The individual counting model (ICM) simultaneously takes into account contributions from excited state lifetime, rotational distribution, and translational motion of the molecule. It is concluded that further study of the systems at several wavelengths in the lowest energy absorption band is necessary to unambiguously characterize the symmetry and electronic coupling of the low-lying excited states of the alkali iodides.

I. INTRODUCTION

The spectra of the low-lying excited states of the alkali halides have been of considerable interest for many years.[1] The interest centers around the question of coupling cases applicable to the states and the curve crossing between ground and excited states. The ionic $^1\Sigma^+$ ground state correlates with ionic products at a dissociation limit above that of the neutral atoms. The excited states of the iodides probed in this work correlate with dissociation to ground state atoms. Under Hund's case (c) coupling,[2] which has generally been assumed to hold for the first excited state of these molecules, Ω is the good quantum number. The state is split into five states designated $\Omega = 2, 1, 1, 0^+$ and 0^-, of which the 2, 1 and 1 states are doubly and the 0^+ and 0^- states singly degenerate. The situation is complicated because the 0^+ and $^1\Sigma^+$ states have the same symmetry and potential curves which cross. Adiabatic curve crossing rules can therefore apply.

The present work applies the photofragment spectroscopic technique[3] to the alkali iodides. A molecular beam of the alkali iodide is crossed with the linearly polarized output of a frequency doubled ruby laser (347.1 nm). Molecules absorbing the light dissociate, and the angular distribution of the recoiling alkali fragment atoms is measured by a surface ionization detector. At the doubled ruby wavelength, there is only enough energy to produce ground state atoms and not excited atoms or ions.

The molecular center of mass coordinate system (CM) is shown in Fig. 1. If the effect of excited state lifetime and molecular rotation is negligible, the distribution in the CM for a one photon transition is given by[4]:

$$w(\theta, \phi) = \frac{1}{4\pi}\left[1 + 2b_0 P_2(\cos\theta)\right] , \tag{1}$$

where θ is the angle between the recoil direction and the polarization vector, ϕ is the azimuthal angle,

$$P_2(\cos\theta) = \tfrac{1}{2}(3\cos^2\theta - 1) \tag{2}$$

is the second degree Legendre polynomial in $\cos\theta$ and b_0 is the so called CM anisotropy factor. b_0 may vary between $-1/2$ and 1. For a pure perpendicular transi-

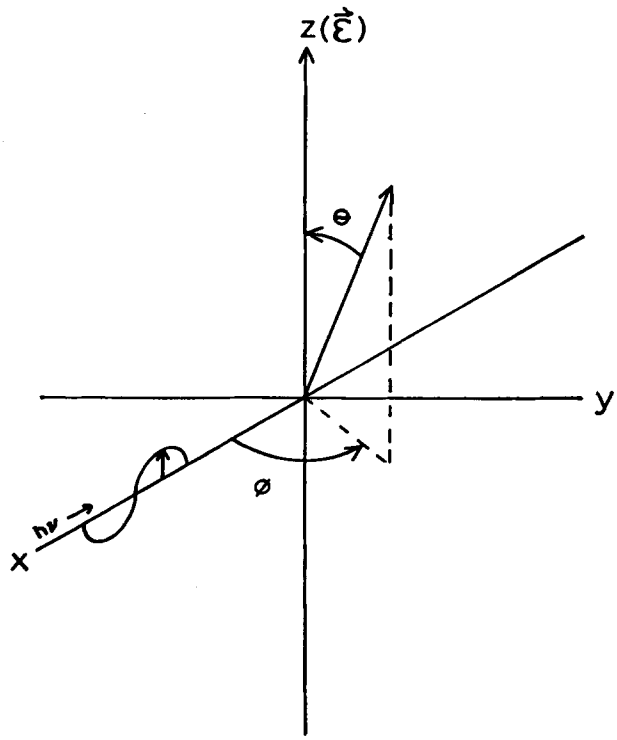

FIG. 1. Center-of-mass coordinate system. The electric polarization vector of the light defines the z axis, while the propagation vector defines the x axis.

[a] Authors to whom correspondence should be addressed.
[b] Present address: Ballistic Research Laboratory, Aberdeen Proving Ground, MD. 21005.
[c] Present address: Brown & Williamson Tobacco Co., 1600 W. Hill Street, Louisville, Ky. 40232.
[d] Present address: EIC Laboratories, Inc., 55 Chapel Street, Newton, Mass. 02158.

 0021-9606/81/063295-12$01.00

tion, $b_0 = -1/2$, while for a parallel transition, $b_0 = 1$. The inclusion of a lifetime necessitates replacement of b_0 by a new shape factor b whose absolute value is closer to the isotropic distribution value of zero.

In order to interpret the experimental results, the effects of translational and rotational motion of the molecules and their excited state lifetime must be considered. Several models to account for these effects on the distribution of Eq. (1) have been published.[5-7] In the course of this work a new model was developed.[8] The model can be used for any CM distribution including saturated and multiphoton distributions. The model, which is presented in the Appendix, is used to aid in the interpretation of the experimental results presented herein.

In this paper, a more detailed description of the experimental apparatus is given than has appeared previously. The data are presented and reduced using the new model. The results are then discussed in terms of the parallel and perpendicular character of the transitions and compared with other studies of the alkali iodides. A preliminary report for KI has appeared[9] as well as a detailed discussion for NaI.[10] The pertinent results from the latter work are included here for comparison with the new results on the other iodides. Generally stated, there is a trend from a highly anisotropic distribution attributable to mostly perpendicular transitions for NaI to a nearly isotropic distribution for RbI and CsI.

During the course of this work, Su and Riley[11] published results on the photodissociation studies of the alkali iodides using 266 nm radiation. LiI produced 100% ground state Li atoms, but excited $I(^2P_{1/2})$ and ground state $I(^2P_{3/2})$ atoms were produced in a 1:2 ratio. The four heavier diatomics dissociated entirely to the ground state alkali atom and the excited $I(^2P_{1/2})$. The transition in LiI leading to ground state atoms was found to be about 70% perpendicular. An even higher perpendicular contribution would have been expected from the trend in our work. However, considering the uncertainties that still exist in interpretation of the experimental results as pointed out in this paper, the results from the two laboratories are in qualitative agreement.

II. EXPERIMENTAL

The apparatus which was described in detail previously by Ormerod[12] was modified by Anderson.[8] As shown in Fig. 2, the experiment centers around a stainless steel scattering chamber evacuated by a six inch diffusion pump with a freon cryobaffle. A beam of the compound of interest was formed by a two stage resistance heated Knudsen type oven at about 1000 K. The beam was collimated by two slits between the oven and interaction zone, the last of which was held by a water cooled plate. A shield placed over the oven reduced radiative heat losses and aided in trapping stray molecules. Chromel-alumel thermocouples inserted through the shield into each stage monitored the temperatures. The primary beam was monitored by a rhenium surface ionization detector[13] (SID) which intercepted the beam below the interaction region. Output of the SID was fed into a digital multimeter operated in the ammeter mode.

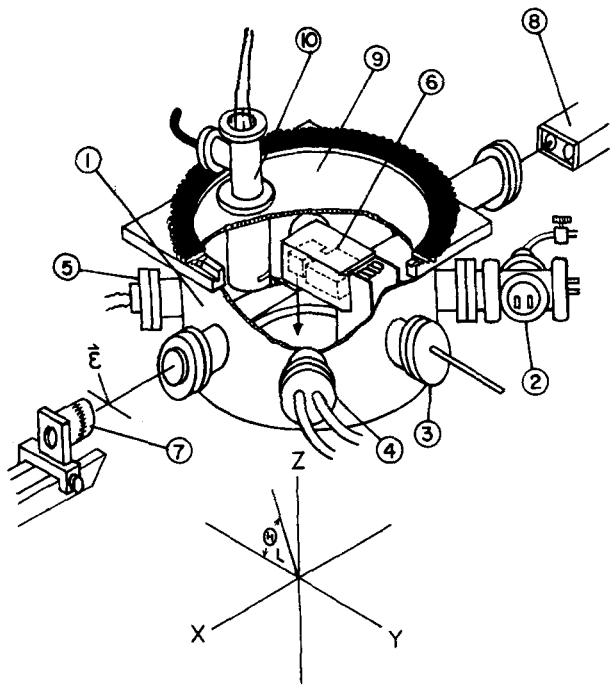

FIG. 2. Cutaway view of scattering chamber. 1. Stainless steel scattering chamber; 2. Feedthrough for gas and oven electrical connections. 3. Feedthrough for beam flag rod. 4. Water feedthrough for cold plate cooling. 5. Electrical feedthrough for thermocouples. 6. Molecular beam oven. 7. Half wave plate at end of laser rail. 8. Calorimeter detector. 9. Vacuum sealed rotatable lid. 10. Upper surface ionization detector.

The linearly polarized output of a Q-switched ruby laser was frequency doubled by a KD*P crystal. The ultraviolet polarization direction was controlled by a half wave plate. The ruby fundamental and any stray polarizations were removed by two glan-air prisms placed between the doubler and half wave plate.

The ultraviolet radiation entered the scattering chamber through a quartz window, crossed the molecular beam at right angles, and exited through another quartz window. The laser beam was intercepted by a calorimeter energy meter. A hard copy of the calorimeter output was obtained on a strip chart recorder. The individual pulse energies were extracted by a procedure described previously.[12]

A typical pulse of uv radiation from the laser had a pulsewidth of 10 nsec FWHM and an energy of 100 mJ. The beam was 0.953 cm in diameter. This power level was not expected to cause significant saturation of the molecular transition, based on the model of Ling and Wilson.[14]

Alkali atoms recoiling perpendicular to the plane defined by the laser and molecular beams were intercepted by a platinum-tungsten alloy SID. The laboratory polarization angle θ_L was defined by the angle between the detector direction and the electric polarization vec-

tor of the light (see Fig. 2). The detector had an angular resolution of 4° FWHM. This acceptance angle was small enough not to significantly perturb the angular distribution.[5,12] The output signal from the SID was fed into a Biomation 610 B transient recorder which was triggered by the laser pulse. The digitized data from the transient recorder were summed in a Nicolet signal averager. Usually, results from 8 shots were accumulated. Then 8 shots were taken with the laser blocked and the resulting background was subtracted from the signal. The signal was integrated in the averager and a hard copy of the signal and its integral were plotted on an X-Y recorder. One such signal from an experiment with RbI is shown in Fig. 3. The arrival time of the leading edge was consistent with the mass of the atoms involved, the energy available for recoil, and the path-length of 10 cm. The shape of the signal was mainly determined by the residence time of the alkali atoms on the detector wire. All of the iodides studied exhibited only a single peak in the arrival time spectra. This result was expected since the single photon energy was only sufficient to produce ground state atoms and not ions or excited atoms.

At least once during each run a beam flag was placed in the beam path to block it from the interaction zone, and the laser was fired. No signal above background was observed under these conditions.

Data obtained at each polarization angle consisted of the average laser pulse energy, the average molecular beam intensity, the photofragment detector signal and its integral. The integral was normalized to correct for changing intensities in the laser and primary molecular beam and plotted against the laser polarization angle. The angles were varied in a random fashion to avoid systematic error.

III. RESULTS

Three runs were made for NaI, which was discussed in a previous letter,[10] four for KI, including two reported previously,[9] four for RbI and two for CsI. θ_L was varied between 0 and 180° for all the runs except run 2 for CsI. For this run θ_L was varied only near the excepted extrema in an effort to observe any anisotropy.

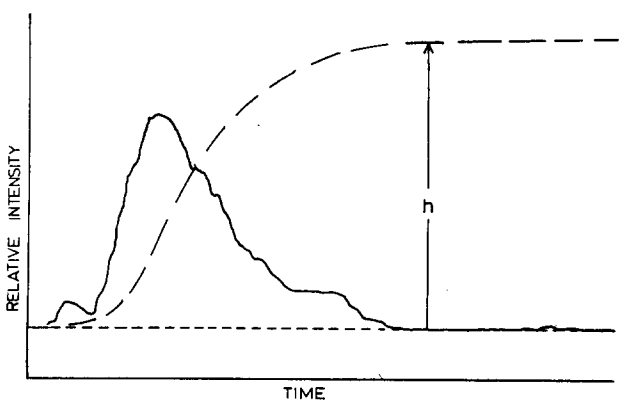

FIG. 3. Typical signal averager output for RbI. Solid curve—rabidium signal. Short dashed curve—baseline. Long dashed curve—integrated rubidium signal.

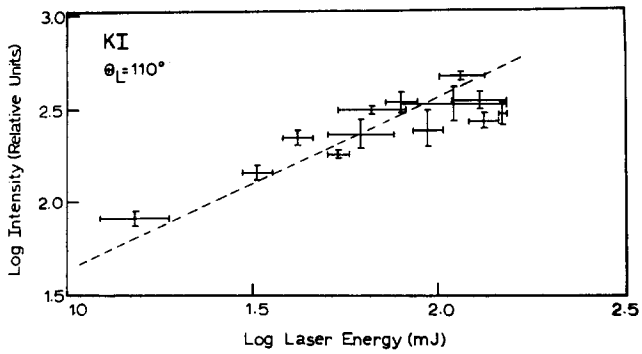

FIG. 4. Log–log plot of potassium atom intensity vs laser energy from KI photodissociation. The signal was measured at $\theta_L = 110°$ which is near the point where the fragment intensity peaks. The dashed line is drawn with a slope of 1.

The new results for KI, which confirm those from the previous work, were obtained with both glan-air prisms set to pass the maximum amount of ultraviolet light possible. In a fifth run on KI one of the glan-air prisms was rotated with θ_L fixed near the expected maximum photofragment intensity for this compound. In this way the incident laser intensity could be varied to check for effects of saturation. For a nonsaturated, one photon transition a log–log plot of detector response vs laser intensity should yield a straight line of slope 1. Such a plot is shown for KI in Fig. 4. While the data are consistent with a slope of 1, their precision is such that this result is far from conclusive. Applying the model of Ling and Wilson[14] using the experimental power levels, however, supports the conclusion that saturation should not be a problem for any of the iodides under our experimental conditions.

The angular distributions obtained from photodissociation of NaI, KI, and RbI were adequate to determine the anisotropy factors. Some typical spectra are given in Figs. 5–7. Only a qualitative indication of the isotropy could be determined from the CsI data because of the low signal levels. Due to their higher mass, the CM recoil velocity of Cs atoms away from the interaction zone is expected to be lower than for the other alkali atoms. In order to obtain sufficient signal, the ovens had to be

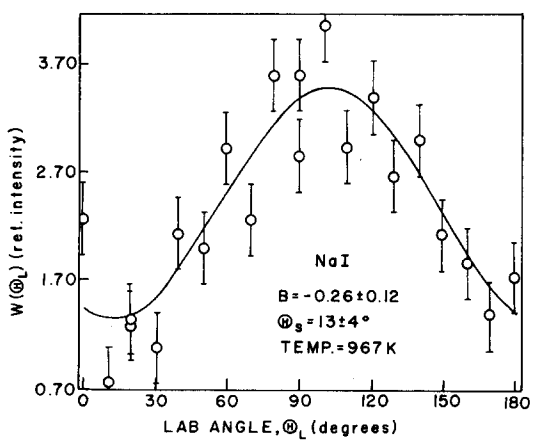

FIG. 5. Normalized sodium intensity vs labroatory angle for NaI run 2. The curve is the fit of the data to Eq. (3).

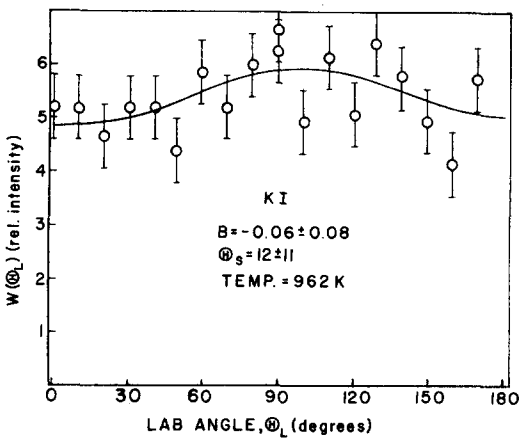

FIG. 6. Normalized potassium intensity vs laboratory angle for KI run 1. The curve is the fit of the data to Eq. (3).

run at a very high temperature. The high temperature resulted not only in a high proportion of the Cs atoms being swept away from the detector by the high velocities of the parent CsI molecules, but also in the ovens running out of beam material very quickly and rapid clogging of the collimating slits. Further attempts to obtain a definitive spectrum from CsI were, therefore, discontinued. The qualitative results, however, indicated a nearly isotropic distribution.

The spectra were fitted to the functional form[7]

$$W(\theta_L) = A\{1 + 2BP_2[\cos(\theta_L - \theta_S)]\}, \quad (3)$$

where A is a proportionality constant, B is the laboratory coordinate system, (LAB) anisotropy factor, and θ_S is the LAB shift angle, that is, the angle between $\theta_L = 0$ and the first extremum in $W(\theta_L)$. Figures 5–7 show the fit of the data to Eq. (3). The average values of B and θ_S for each compound are listed in Table I. The results indicate a highly anisotropic distribution corresponding to mostly perpendicular transition for NaI, becoming nearly isotropic for RbI and probably isotropic for CsI. The error in θ_S becomes very large as isotropy is approached as is expected since the distribution is nearly a horizontal line.

TABLE I. Laboratory shape factor B and shift angle θ_s for experimental photofragment distribution of alkali iodides.

Molecule[a]	T (°C)[b]	B	θ_s (deg.)
NaI (3)	684–704	-0.32 ± 0.09	13 ± 6
KI (4)	662–692	-0.10 ± 0.06	25 ± 6
RbI (4)	640–750	0.04 ± 0.13	20 ± 10
CsI (2)	713–761	$\simeq 0$	...

[a]Number in parenthesis indicates number of runs for each system.
[b]Temperature of front chamber of oven generating molecular beam.

IV. DISCUSSION

A. Dynamic model to calculate laboratory angular distributions

1. General approach

The CM distribution of photofragments becomes less anisotropic when account is taken of the excited state lifetime and molecular rotation. Furthermore, the molecular beam translational velocity not only broadens the observed angular distribution still further but also shifts the angle of maximum intensity.[5,7] In order to interpret the observed photofragment spectra of the alkali iodides in terms of the molecular transition probabilities in the CM system, the relative probability of observing a photofragment at a given θ_L is calculated by summing over the individual probabilities of each possible combination of lifetime, rotational state and CM translational velocity which can reach a detector of infinite resolution. The model is therefore called the individual counting model (ICM). For the first time the CM to LAB transformation has been performed in one step rather than by separating the individual effects as was done in previous models.[5–7,12] The model is applied here to Eq. (1), but it is applicable to any CM distribution including those arising from saturated and multiphoton processes. The effect of the finite resolution of the detector, as stated previously, has been ignored because of its small acceptance angle.

A detailed derivation of the ICM is given in the Appendix. The general approach of the model is outlined here along with several figures to help visualize the coordinate systems and associated transformation. Initially, a lab angle θ_L is selected. The orientation of the molecule at the instant of absorption is arbitrarily chosen. The recoil velocity of the detected fragment in the CM in the presence of rotation is defined as $\mathbf{u}$ (see Fig. 14). The $\mathbf{u}$'s which are considered are restricted to that subset whose directions allow detection (Fig. 12, see Appendix). A $\mathbf{u}$ direction is arbitrarily chosen from this subset. $\mathbf{u}_0$ is defined as the CM recoil velocity without the effects of rotational deflection. A direction of $\mathbf{u}_0$ is chosen which lies in the plane formed by $\mathbf{u}$ and the bond axis at the starting molecular position. It is assumed that the molecule rotates through an angle $\psi \pm 2\pi n$ ($n = 0, 1, 2, \ldots$) between the bond axis in the starting molecular position

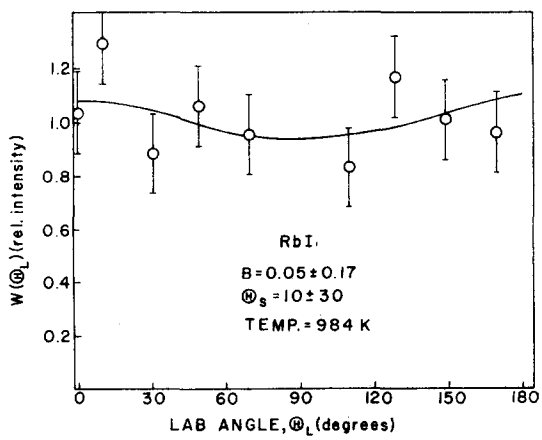

FIG. 7. Normalized rubidium intensity vs laboratory angle for RbI run 4. The curve is the fit of the data to Eq. (3).

and u_0 during its excited state lifetime (Fig. 14). The molecule then dissociates with tangential velocity v_t adding to u_0 and therefore deflecting the fragment path along u. Since the tangential velocity is determined by the deflection angle, the magnitude of u is determined. As seen in Fig. 12, only one CM translational velocity c will add to u to give a LAB recoil velocity vector v which must point towards the detector.

The individual detection probability P_1 due to the most acute lifetime angle $\psi_{1,0}$ is formed by multiplying its probability by (1) the probability of α which is the rotational deflection angle between u and u_0, (2) the probability of the c necessitated by the u, (3) the absorption probability, and (4) several solid angle and detector velocity dependent terms. The probabilities of the rest of the Ψ's are totaled and treated in a similar fashion to form detection probability P_2. The reason for the separation into contributions P_1 and P_2 is that different integration limits are necessary for the two contributions to the intensity (see Appendix).

The convolution is performed in the following manner. The total probability P_T of detection for a selected u direction and molecular position is determined by integrating P_1 and P_2 over their respective limits in α and summing the integrals. P_T is then integrated over all possible starting molecular orientations to find P_D the total probability of dissociation in the u direction. Finally, P_D is integrated over the subset of u directions for which detection may occur. This integral is assumed to be proportional to the total probability of detection $W(\theta_L)$ at the angle θ_L. Generation of $W(\theta_L)$ as a function of θ_L provides a LAB angular distribution. θ_S and B may be determined from the generated distribution and compared with experimental results.

The application of the ICM to a number of diatomic systems for which there is experimental data has been discussed elsewhere.[8] The results were also compared with those for other dynamic models. To summarize briefly, the ICM gives values in better agreement with the experimental results for θ_S than did the model presented by Ormerod.[12] A separation of the dynamic effects for rotation and lifetime allowed comparison with the Yang and Bersohn model.[6] Excellent agreement was found between the two models for the anisotropy as a function of excited state lifetime. As the lifetime is increased in the ICM, the laboratory B approaches a limiting value slightly less than $1/4b_0$. Presumedly, the effect of infinitely long lifetime reduces the magnitude of b to $1/4b_0$, in agreement with two previous models.[5,6] The effects of translational motion of the molecular beam and rotational deflection of the recoiling atoms reduce the magnitude of B to slightly less than $1/4b_0$. Furthermore, an isotropic distribution in the CM yields an isotropic distribution in the LAB, a most comforting result. However, the ICM results for intermediate lifetimes did not agree as well with those obtained using the model proposed by Busch and Wilson.[5] Significantly, the ICM did not yield their hard-to-rationalize result that for some high rotational velocities the anisotropy *increases* from the zero lifetime limit as the mean lifetime increases.

TABLE II. Constants used in the ICM calculation.

Molecule	D_e (eV)[a]	ω_e (cm^{-1})[a]	E_t (eV)	$\hat{u}_0$	R_e (Å)[b]
NaI	3.15	258	0.43	5.19	2.71
KI	3.33	173	0.23	3.01	3.05
RbI	3.29	128	0.30	2.20	3.18
CsI	3.37	101	0.22	1.49	3.32

[a]From Ref. 15. [b]From Ref. 16.

TABLE III. Angular distributions constants predicted by the ICM for the alkali iodides.[a]

Molecule	b_0	B	θ_S (deg.)
NaI	1.0	0.95	12
	−0.5	−0.46	13
	−0.35	−0.32[b]	13
KI	−0.5	−0.42	22
	−0.12	−0.10[b]	22
RbI	−0.5	−0.37	29
	0.06	0.04[b]	29
CsI	−0.5	−0.29	39

[a]The assumed temperature was 1000 K and lifetime time of the excited state was 0.001 psec. Changing the assumed temperature over the experimental temperature ranges does not alter the predicted distributions appreciably. The zero lifetime limit in the observed distributions is reached at 0.001 psec.
[b]Experimentally observed B value.

2. *Application of the ICM to the alkali iodides*

Application of the ICM to the alkali iodides is of particular interest in the present work. As the lifetime τ and b_0 are varied, the value of B varies between −0.5 and 1.0 while the value of θ_S is nearly constant. All the information on excited state symmetries and lifetime is therefore carried in the single factor B. With the help of the available spectroscopic data, however, it is often possible to extract a unique transition symmetry which leads to the observed distribution.

The quantities in Table II were used with the ICM to calculate the value of B and θ_S for each compound at 1000 K for several limiting values of b_0 at the negligible lifetime $\tau = 0.001$ psec. The dissociation energies D_e and vibrational frequencies ω_e from Ref. 15 were used to estimate the amount of energy available E_t for translation of the products and the magnitude of $\hat{u}_0$, the reduced recoil velocity (see Appendix). The equilibrium internuclear distances R_e from Ref. 16 were used to estimate the effects of rotational motion. The values of B and θ_S resulting from the assumed b_0 are presented in Table III. The predicted θ_S values for NaI, KI, and RbI of 13°, 22°, and 29° agreed very well with the experimental values of 13±6, 25±6, and 20±10°, respectively. The value of b_0 which produced the experimentally observed B at negligible lifetimes is also shown in the table. If direct (zero lifetime) dissociation is assumed, the b_0 which produced the experimental result

for NaI and KI in the ICM was in fair agreement with that calculated by Su and Riley[11] using the model of Busch and Wilson. The CM distribution predicted by their model, however, was slightly more anisotropic than that from the ICM.

An estimate of the effects of lifetime on purely repulsive (diabatic) excited states was made by first estimating the separation time of the two atoms. The excited state potentials derived from the absorption data of Davidovits and Brodhead[17] were used to estimate the time taken by the atoms to reach 90% of their final velocity.[8] Use of these longer "lifetimes" in the ICM showed that the effect on the observed B and θ_S were very small.

For adiabatic states ($\Omega = 0^+$), the situation is much more complicated. An estimate of the probability of dissociation on a given vibration is made by considering the Landau–Zener transition probability[18] using the potential splittings of Herschbach and Grice.[19] The probabilities of dissociation calculated for NaI, KI, RbI, and CsI were 1.8, 93, > 99 and > 99%, respectively.[8] For NaI this transition probability led to such a long lifetime (at least 12 psec) that the $1/4b_0$ limit was easily reached, while for RbI and CsI the short lifetime limits applied. If the Landau–Zener model is quantitatively correct, KI is also expected to follow the short lifetime limit. Su and Riley[11] showed that a lifetime of 0.5 psec, which is much longer than expected if most of the molecules dissociate on the first vibration, leads to a simple interpretation of our results at 347 nm and theirs at 266 nm. It is doubtful that such a long lifetime is realistic, however, and the results presented here are interpreted on the basis of the short lifetime limits. Validity of our assumption for KI, of course, rests on the applicability of the Landau–Zener model and the accuracy of the splitting calculations. For the other two molecules, the limiting case for "zero" lifetime is surely applicable.

B. Angular momentum coupling

The discussion to this point has assumed applicability of Hund's case (c) coupling to the alkali iodides. However, a recent spin depolarization study by Carter and Pritchard[20] suggests that, at least for KI, Hund's case (c) does not apply. They suggest type J–J coupling occurs, which is similar to j–j coupling in atoms. An overall molecular angular momentum quantum number J_M results with allowed values $J_M = 2$ (fivefold degenerate) and 1 (threefold degenerate). Only $1 \leftarrow {}^1\Sigma^+$ transitions are optically allowed. As Berry[1] points out, however, transitions to the 1 state could be of mixed parallel-perpendicular character, making it impossible to determine from the photofragment distribution at only one wavelength which type of coupling applies. The results of the atomic beam scattering studies of Kaufman *et al.*[21] on the KI system were not fit well using only two excited state potentials. Their work would seem to be evidence in favor of Hund's case (c) coupling.

Berry suggests that J–J coupling could occur for the high rotational levels at large internuclear separations probed in the spin depolarization study.[1] At the energy and impact parameter in the Carter and Pritchard study of 0.21 eV and 4.2 Å, respectively, the rotational level excited would be ~ 200, if the KI were bound. The splitting between adjacent levels is ~ 20 cm^{-1}, which might be greater than the splitting between Ω levels at 4.2 Å[21] and might result in type J–J coupling.

Another way of looking at the coupling is that at large internuclear distances the electric field between the nuclei is weak. If the rotational angular momentum is large, the electronic angular moments might couple to it rather than the internuclear axis. Such coupling might occur even in the photodissociation experiments as the nuclei separate. However, this type of coupling does not seem likely near the repulsive portion of the potential curve since the electric field is strong. Due to the Franck–Condon principle, coupling near this portion of the potential will govern the absorption symmetry. Crossover to J–J coupling should not significantly affect the nuclear motion. Therefore, for the purposes of interpretation of the present study, Hund's case (c) coupling will be assumed. As will be seen, the assumption of case (c) coupling only enters into the calculation of the parallel–perpendicular character from the photodissociation data for NaI since its $\Omega = 0^+$ excited state has a nonnegligible lifetime.

C. Interpretation of B values

1. *Sodium iodide*

As the results for the NaI photodissociation were the subject of a previous report,[10] only the major results will be summarized and discussed in light of new work. The average experimental B value for NaI is -0.32 ± 0.09. For negligible lifetimes, the b_0 which would produce this result is -0.35 ± 0.10 (see Table III). Using the equation $b_0 = \chi_{\parallel}(1.0) + (1 - \chi_{\parallel})(-0.5)$ where $\chi_{\parallel}$ is the fraction contributed by parallel transitions, we find this b_0 corresponds to $10 \pm 7\%$ parallel transitions.

If Hund's case (c) applies, however, the situation for NaI is complicated by the avoided adiabatic curve crossing of the 0^+ and ${}^1\Sigma^+$ states. If the 0^+ state's contribution to the photofragment distribution has proceeded to the long lifetime limit, as seems likely from the discussion in Sec. IV A. 2, its b_0 would have to be replaced by $b = 1/4b_0$. The equation for the calculation of the relative perpendicular and parallel contribution becomes $b = \chi_{\parallel}(0.25) + (1 - \chi_{\parallel})(-0.5)$ and gives a $20 \pm 12\%$ parallel transition for the b value, which yields the experimental B value. This we believe to be the most reasonable interpretation of our result.

The analysis reported previously[10] assumed that the $0^+ \leftarrow {}^1\Sigma^+$ transition would be fully parallel and the $1 \leftarrow {}^1\Sigma^+$ fully perpendicular. However, the individual transitions cited above could be of mixed character, leaving an exceedingly complicated situation.[1] The proper equation to use for b then becomes $b = [\chi_{\parallel,0} + (0.25) + (1 - \chi_{\parallel,0} +)(-0.125)] + [\chi_{\parallel,1}(1.0) + (1 - \chi_{\parallel,1})(-0.5)]$, where $\chi_{\parallel,0} +$ and $\chi_{\parallel,1}$ refer to the fraction of parallel transitions to the 0^+ and 1 state, respectively. Since determination of the two unknowns is not possible from our data, this discussion assumes that the transitions are not mixed. The question of mixed transitions, however, remains to be studied.

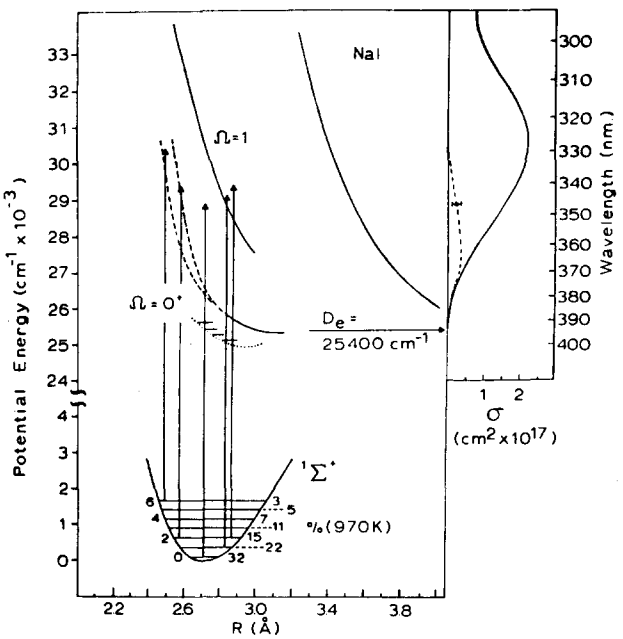

FIG. 8. Potential energy diagram and absorption curves for sodium iodide. The arrows drawn are 3.57 eV long, the energy used in this work. The ground state vibrational population distribution at 970 K is shown. The curve labeled $\Omega = 1$ was deconvoluted from the absorption curve of Davidovits and Brodhead (Ref. 17), the latter curve being shown as the solid line at the right of the figure. The excited state curve whose repulsive portion lies at large R is from the crossed molecular beam work of Delvigne and Los (Ref. 22) and is probably a composite of all the excited state curves. The dotted curve is suggested by the matrix isolation experiments of Oppenheimer and Berry (Ref. 24). The curve labeled $\Omega = 0^+$ is the combined result of the experiments of Levi and of this work. The solid portion of the curve is due to Levi (Ref. 23) while the two dashed curves bracket the range of the potential suggested in this work. The dashed curve and point under the absorption curve are the absorption curve to the $\Omega = 0^+$ state suggested by this work.

The present state of understanding of the low-lying electronic states of NaI is summarized by the potential energy diagram in Fig. 8 and was discussed previously.[10] The curve labeled $\Omega = 1$ is the potential arising from deconvolution of the absorption spectrum.[17] The excited state curve whose repulsive portion lies at large R is that which results from a molecular beam study of the reaction $Na + I \rightarrow Na^+ + I^-$.[22] The solid portion of the $\Omega = 0^+$ curve is suggested by the work of Levi.[23] The dotted curve is suggested by Oppenheimer and Berry from their low temperature matrix isolation experiments.[24] They state their results are consistent with placement of the minimum in the 0^+ potential directly over that in the ground state potential.

Our previous analysis of the NaI photodissociation spectrum led to the conclusion that the transition moment appears to be substantially less to the 0^+ state than to the 1 state. Berry has offered an alternative suggestion for our results.[1] A many-lined spectrum has been observed for NaI[25,26] which suggests the 0^+ state is quasibound with vibrational spacing 35 cm^{-1}. Berry pointed out the possibility that the line at 347.1 nm may fall between absorption lines to the 0^+ state and excite only the underlying 1 continuum. Su and Riley[11] suggested this is the reason for the highly perpendicular transition. However, the ruby laser line is 5.3 Å wide, or 11 cm^{-1} at 694.3 nm.[27] Upon doubling, the line must be approximately twice this wide, i.e., 22 cm^{-1}. Due to the high density of states expected for such a heavy molecule in all electronic states, it seems unlikely that transitions to the 0^+ state could be missed. Nevertheless the $0^+ \leftarrow {}^1\Sigma^+$ transition at 347.1 nm could involve vibrational bands with small transition probabilities. Resolution of this question must await a detailed analysis of the many-lined spectrum.

Assuming pure perpendicular and parallel transitions to the 1 and 0^+ states, respectively, and continuous absorption by the 0^+ state, the absorption curve for the 0^+ state *alone* looks something like the dashed curve at the right of Fig. 8. The point shows the absorption due to 0^+ contribution at 347.1 nm. Parallel transitions to 0^+ would predominate at long wavelengths and perpendicular transitions to 1 at shorter wavelengths. If the 0^+ absorption is structured, the absorption curve to this state would be a dense line spectrum, but probably would retain the same general envelope as the continuum depicted.

2. *Potassium iodide*

The average experimental B value for KI is -0.10 ± 0.06. As indicated by the Landau–Zener transition theory and the ICM, the excited state lifetime probably has a negligible effect on this result. Thus, the b_0 which produces this result is $b_0 = -0.12 \pm 0.07$ in agreement with our earlier published result.[9] Since excited state lifetime and curve crossing are not expected to complicate the picture, we have the equation $b_0 = \chi_{\parallel}(1.0) + (1 - \chi_{\parallel})(-0.5)$ or $\chi_{\parallel} = 25 \pm 5\%$.

Let us consider the meaning of the fraction of parallel transitions in terms of the potentials for KI. The present state of understanding of the low-lying potentials of KI is summarized in Fig. 9. Not considered here are potentials resulting from two crossed atomic beam studies[28,29] whose minima lie so far to the right of the ground state minimum that it is difficult to see how they could contribute to the lowest energy KI absorption band.[8] The potentials arising from the crossed atomic beam study[21] are depicted in the figure. Results of this study should be more sensitive to the shape and placement of the potential minima than the other studies since wide angle scattering at low translational energies was considered.[8] The circles shown in the figure result from deconvolution of the absorption spectrum, assuming equal Franck–Condon factors for each vibrational state. A smooth curve was drawn through the circles. The experimental absorption spectrum[17] is depicted to the right. The dashed curve is the result of a flame emission study by Kaufman *et al.*[30] The ground state potential is a truncated Rittner potential.[31] Arrows drawn in the diagram correspond to the photon energies of 3.57 eV used in this work.

In the atomic beam study[21] the Lennard-Jones form was assumed for the excited state potentials. The curves labelled $\Omega = 0^+$, $\Omega = 1$, $\Omega = 0^-$, ?, and Ω = ? have

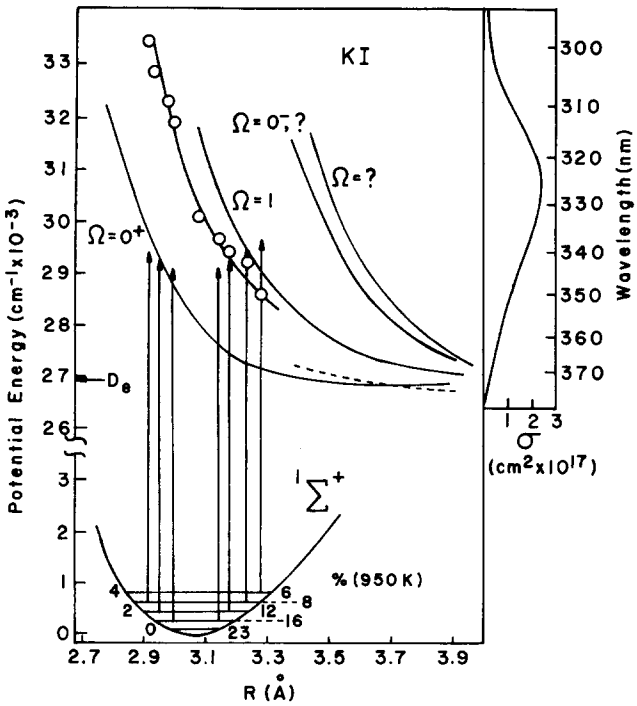

FIG. 9. Potential energy diagram and absorption curves for potassium iodide. The arrows drawn are 3.57 eV long, the energy used in this work. The ground state vibrational population distribution at 950 K is shown. The circles are points deconvoluted from the absorption spectra of Davidovits and Brodhead (Ref. 17), the absorption spectra being shown at the right. A smooth curve is drawn through the circles. The dashed curve results from flame emission experiments (Ref. 30). The four solid curves result from crossed atomic beam experiments (Ref. 21). The statistical weights of the curves labeled 0^+; 1; 0^-, ?; and ? are 1, 2, 3, and 2, respectively.

statistical weights 1, 2, 3, and 2, well depths 150, 26, 85, and 130 cm^{-1} and dissociation limit crossing points of 3.43, 4.29, 4.29, and 4.25 Å, respectively. At least four potentials were necessary to explain the observed scattering data. If transitions to the 0^+ state are 100% parallel and to the 1 state 100% perpendicular, the curves must be labelled as shown in Fig. 9 because both transition types are observed at 3.57 eV in the present work. Transitions to the other curves are not likely at this energy and the statistical weights do not allow the reverse assignment.

Oppenheimer and Berry did not observe *any* absorption by KI in their matrix isolation experiments. This result is expected since KI is predicted to follow the diabatic potentials. The absorption is continuous and probably too broad to observe above background in the matrix isolation experiments.[24] This hypothesis is consistent with the failure to observe absorption in matrix isolated NaI at short wavelengths where transitions to the 1 state would be important.

The contributions to the absorption curve for KI from transitions to the individual 0^+ and 1 states is not so clear cut as that for NaI. Due to the high population of excited vibrational levels, transitions at the peak of the absorption curve at 325 nm could easily occur from either turning point of the ground state to the 0^+ and 1 states as shown in Fig. 9. With increasing photon energy, transitions to the 1 state are expected to dominate as was predicted for NaI. However, in contrast to the NaI system, as the photon energy is decreased, transitions are expected to occur from the right turning point and be mixed because the excited states lie so close to one another.

3. *Rubidium iodide and cesium iodide*

The average experimental B value for RbI at 3.57 eV was 0.04 ± 0.13 (see Table I). The experimental B value for CsI could not be determined. However, the experimental results seem to indicate a near isotropic distribution, since there was little difference in the observed Cs intensity near the expected minimum and maximum in the distribution.[8] The b_0 which gives the experimental B value for RbI is 0.06 ± 0.20. This b_0 gives a 36 $\pm$13% parallel transition. The near isotropic distribution for CsI corresponds to a transition of approximately 33% parallel character.

The present understanding of the low-lying states of RbI and CsI is summarized in Figs. 10 and 11, respectively. As can be seen, there is a dearth of information about these compounds. Ewing, Milstein and Berry's collisional dissociation work[31] suggests that these compounds behave diabatically, as predicted by the Landau–Zener theory. The only measurements from which the excited state potentials may be deduced are absorption measurements such as those of Davidovits and Brodhead,[17] shown at the right of the figures. The ground states are truncated Rittner potentials.[32] The RbI excited potential is derived from the absorption data in a

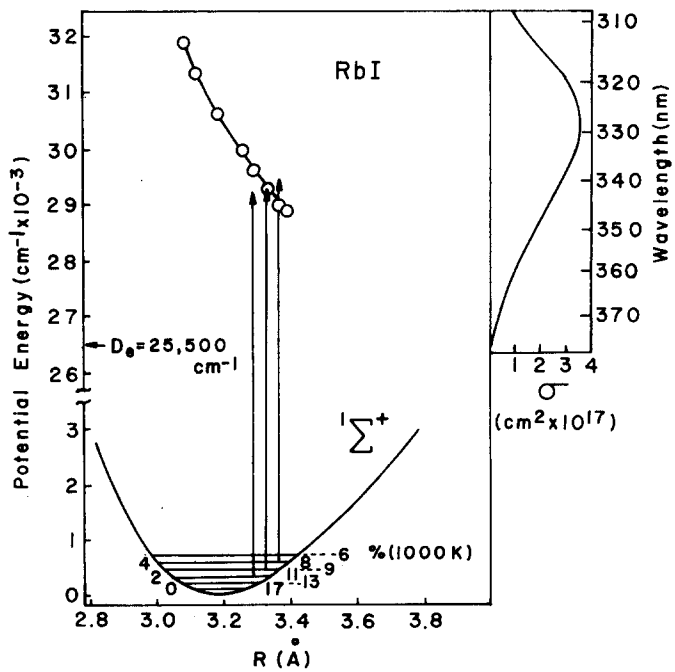

FIG. 10. Potential energy diagram for rubidium iodide. The arrows drawn are 3.57 eV long, the energy used in this work. The vibrational ground state population at 1000 K is shown. The circles were deconvoluted from the absorption data of Davidovits and Brodhead (Ref. 17) shown at the right. A smooth curve is drawn through the circles.

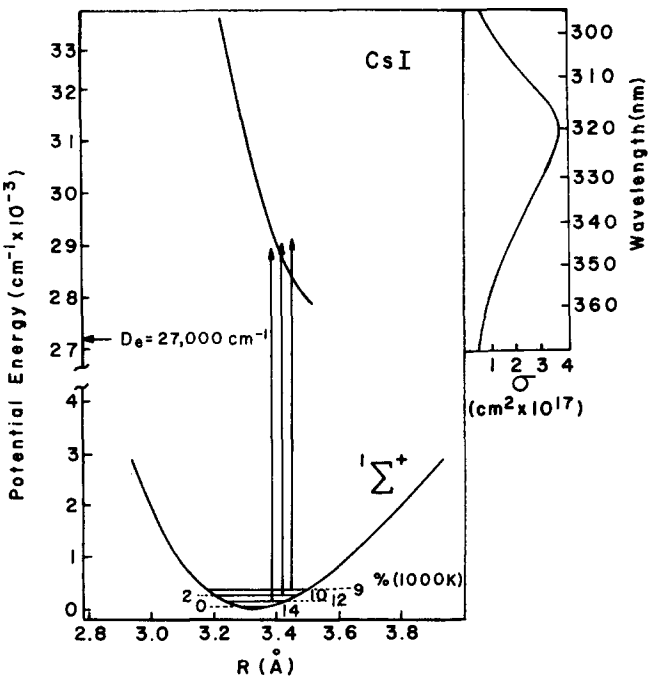

FIG. 11. Potential energy diagram for cesium iodide. The arrows drawn are 3.57 eV long, the energy used in this work. The vibrational ground state population at 1000 K is shown. The excited state potential was derived by Davidovits and Brodhead (Ref. 17) from their absorption spectra shown at the right.

manner similar to that used for KI. The CsI excited potential is taken directly from the work of Davidovits and Brodhead. Transitions at 3.57 eV can occur as shown in the figures. Lacking knowledge of placement and splittings of the excited state manifold, it is difficult to predict anything about trends in the perpendicular : parallel ratio of the transition with changes in excitation wavelength.

V. CONCLUSION

Photofragment spectroscopic experiments have been performed at 347.1 nm for NaI, KI, RbI, and CsI. The results indicate a trend from a highly anisotropic, mainly perpendicular transition for NaI to a nearly isotropic distribution for RbI and CsI. If excited state lifetimes are unimportant for KI, RbI, and CsI, as predicted by the Landau–Zener theory, the results indicate 25 ± 5, 36 ± 13, and ~33% parallel transitions, respectively. For NaI, the discrete absorption spectrum suggests Hund's case (c) applies, and if the $0^+ \leftarrow {}^1\Sigma^+$ and $1 \leftarrow {}^1\Sigma^+$ transitions are also purely parallel and perpendicular, respectively, then the results indicate $20 \pm 12\%$ parallel transitions occur. Even if the above transitions are not pure, one can unabiguously conclude that some absorption to the $\Omega = 1$ state must occur to give such a high negative B value. Transitions to the 0^+ state need not occur to explain the results, although their exclusion seems unlikely due to the laser linewidth. The agreement between the shift angle calculated using the ICM and the experimental results of this work is much better than with the results of a previous model.[12] The agreement for the low-lying transitions in this work also appears better than that achieved using the Busch and Wilson model to interpret results of experiments on higher lying transitions of the alkali iodides.

From the relative parallel : perpendicular transition strengths at 266 nm, Su and Riley calculated the expected relative strengths at 347.1 nm. The assumption was made that since dissociation at 266 nm produces excited I atoms and twice as many $\Omega = 2$ states correlate to ground state I atoms as excited I atoms, absorption at 347.1 nm would have twice the relative perpendicular character. The calculated values agreed well with the experimental results for RbI and CsI, but poorly for NaI and KI. The 0.5 psec lifetime for the excited 0^+ state of KI which the authors used to explain the discrepancy seems unrealistically long (see Sec. IV A.2). For the case of NaI no adjustment of the lifetime could reconcile the difference. Considering the possibility of mixed character in transitions between the individual states, the lack of a clear understanding of the coupling schemes involved, the possibility of a wavelength dependence of the parallel : perpendicular ratio, and for NaI, the question of the effects of the discrete spectrum, it is not surprising that the simple model does not work well. Since several of the problems cited above pertain to RbI and CsI as well, the agreement reported by Su and Riley may be fortuitous.

Experiments at more than one wavelength leading to ground state products may allow unambiguous determination of which coupling case is applicable to each molecule. It would be very interesting to use a tunable laser to investigate NaI to see if structure due to the 0^+ state is present in the photodissociation spectrum vs wavelength. Such devices are capable of achieving linewidths of 0.1 cm^{-1}, which might be adequate resolution if only one vibrational band is excited. Angular distribution data on and off absorption peaks, if observed, would be extremely useful. Similar experiments on the other iodides would also be interesting. If J–J coupling obtains at the time of absorption, only transitions to the $J_M = 1$ state are allowed and the ratio of parallel : perpendicular transitions should be independent of wavelength. For Hund's case (c) coupling, the ratio should vary with wavelength since the 0^+ and 1 curves are split.

It is suggested that if further photodissociation experiments of the type described in this study are contemplated, some variant of the single atom detection technique employed by Grossman *et al.*,[33] be considered. Cs atoms were photoionized in a two step resonant process and detected using a proportional counter. Beam experiments might involve use of a second laser beam crossing the interaction zone coincident with the dissociation laser beam or probing at some point in space a short time after the dissociation pulse. Ions could be detected by an electron multiplier. Flight paths of the ions should not be significantly different from those of the atoms provided space-charge effects are not too large. This method appears to be much more sensitive than mass spectrometric or surface ionization techniques and could make feasible use of much lower molecular and photodissociation laser beam fluxes.

ACKNOWLEDGMENTS

The authors would like to acknowledge Dr. Phil Brooks for many helpful discussions, Dr. Thomas Ridgeway for help in design of the electronics, and Paul Brigham for his assistance in gathering data. The authors gratefully acknowledge the Robert A. Welch Foundation and the National Science Foundation for partial support of this work.

APPENDIX: INDIVIDUAL COUNTING MODEL

The following is the specific formulation used in the ICM. Consider, first, u_0 the translation recoil speed of a fragment in the CM in the absence of rotation. The translational energy of the fragments is

$$E_t = h\nu + E_v - D_e - E_{\text{int}} \ , \tag{A1}$$

where $h\nu$ is the photon energy, E_v is the vibrational energy of the parent molecule, D_e is the dissociation energy, and E_{int} is the internal energy of the fragments. u_0 is derived using the conservation of linear momentum in the CM,[4] and is given by

$$u_0 = \frac{1}{m_1}(2E_t\mu)^{1/2} \ , \tag{A2}$$

where m_1 is the mass of the recoiling fragment and μ is the reduced mass of the molecule. The reduced recoil speed is defined by

$$\hat{u}_0 = u_0/\kappa \ , \tag{A3}$$

where the caret indicates division by κ

$$\kappa = (2kT/M)^{1/2} \ , \tag{A4}$$

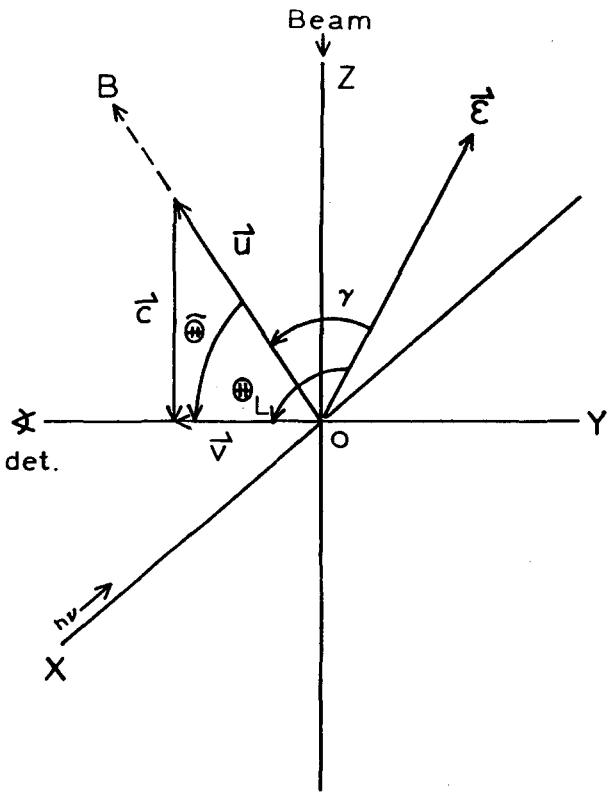

FIG. 12. Velocity vector diagram in the laboratory coordinate system.

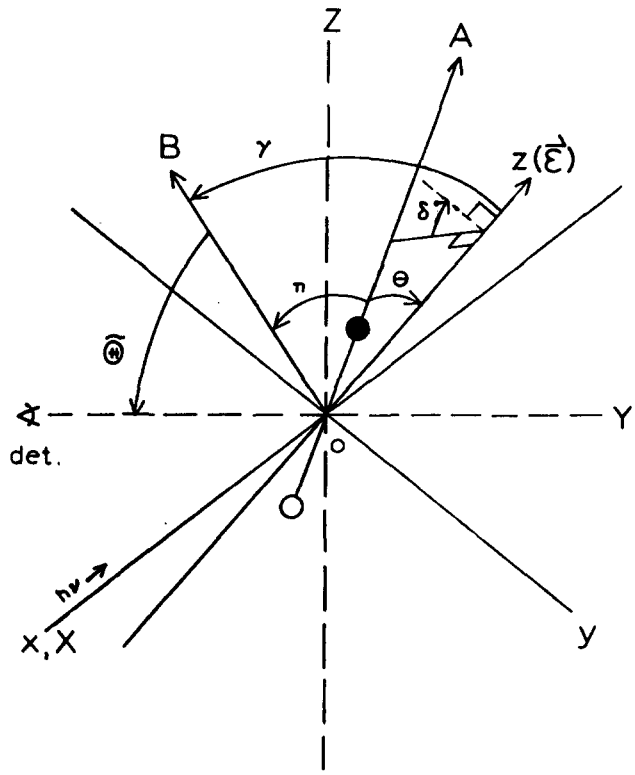

FIG. 13. Geometric relation of OA and OB in the LAB and CM. The molecule is shown at its position of absorption with detectable and undetectable fragments represented by the filled and unfilled circles, respectively. Ray OA does not necessarily lie in any of the planes formed by the LAB and CM axes.

the most probable speed in the molecular beam. Here, T is the beam temperature, k is the Boltzmann constant, and M is the parent molecular mass.

Figures 12, 13, and 14 show how lifetime, rotation and translation couple the initial molecular position and direction to the LAB recoil velocity **v**. The LAB is shown with velocity vectors in Fig. 12. A linearly polarized light beam is directed along the X axis and the molecular beam along the Z axis. $\tilde{\theta}$ is the angle between **v** and **u** and the difference betwwen θ_L and $\tilde{\theta}$ is defined as γ. Since the molecular beam is directed normal to the XY plane, **c** must also be normal to the plane and perpendicular to **v**. The magnitude of **c** is given by

$$c = u\sin\tilde{\theta} \ . \tag{A5}$$

The direction of **u** defines the line OB referred to in the paper as the arbitrarily selected direction for which detection is allowed. Note that since **c** is normal to the XY plane, OB must lie in the YZ plane if detection is to occur. In addition, unless $0 \le \tilde{\theta} \le \pi/2$ detection cannot occur.

In Fig. 13, the situation is considered from the CM viewpoint. The z axis is defined by the electric vector and the x axis by the direction of propagation of the light. Since the x and X axes are coincident, yz and YZ define the same plane. In other words, the transformation involves a rotation of the YZ plane around the X axis. Suppose a molecule lies on arbitrary ray OA (which need not necessarily lie in *any* of the planes

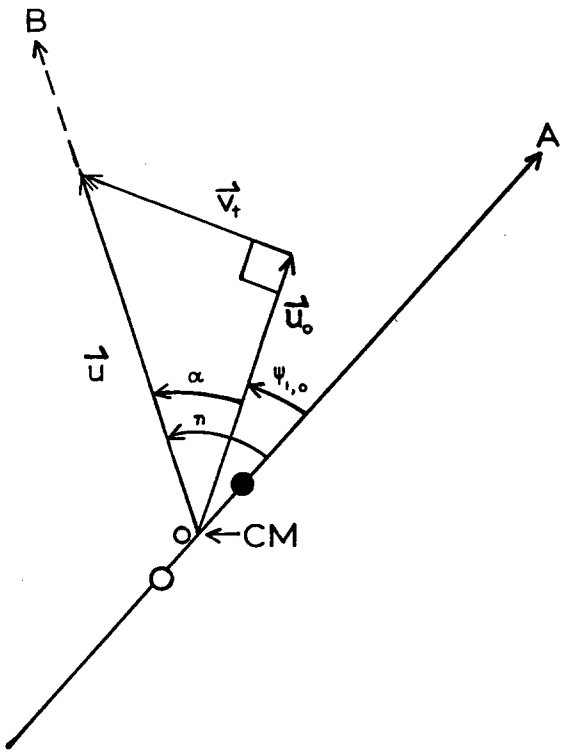

FIG. 14. Velocity vector diagram for the excited state lifetime and rotational deflection effects. The diagram shows how fragment recoil along 0B may result after absorption at 0A. The detectable fragment is represented by the filled in circle. CM denotes the molecular center of mass.

formed by the three axes) with the detectable fragment pointing toward A. This direction defines the arbitrarily selected molecular position. η is defined as angle AOB and δ as the dihedral angle between the yz plane and the AOz plane. Referring back to Fig. 12, the angle in Fig. 13 between OB and the electric vector $\epsilon(=z)$ is γ. In the absence of excited state lifetime and rotational deflection, recoil would occur along OA. Therefore, in order to be able to use Eq. (1), θ is defined as angle AOz. Angle η is expressed in terms of γ, θ, and δ. A tedious but straightforward derivation shows that

$$\eta = \arccos(\sin\theta\cos\delta\sin\gamma + \cos\theta\cos\gamma) \ . \tag{A6}$$

The probability P_T that a molecule starting at arbitrarily selected OA will have a recoil velocity direction along OB and thus be detected is now calculated. Consider a molecule lying on OA as shown in Fig. 14. After the molecule has absorbed a photon, it rotates through some angle $\psi_{i,l}$ during its excited state lifetime. It then dissociates. The angle between $\mathbf{u}$ and $\mathbf{u}_0$ is α. $\mathbf{v}_t$ is the rotational tangential velocity at the time of dissociation. Thus

$$u = u_0/\cos\alpha \ . \tag{A7}$$

In order for detection to occur (see Fig. 12), we must have

$$c = u\sin\tilde{\theta} = u_0\sin\tilde{\theta}\cos\alpha \tag{A8}$$

and

$$v = u\cos\tilde{\theta} = u_0\cos\tilde{\theta}\cos\alpha \ . \tag{A9}$$

If an α is arbitrarily selected between 0 and $\pi/2$, recoil occurs along OB if the molecule rotates in one direction through lifetime angle $\psi_{1,0}$ or $2\pi+\psi_{1,0},\ldots$. Thus,

$$\psi_{1,l} = 2\pi l + \eta - \alpha \ , \quad l = 0, 1, 2, \ldots \ . \tag{A10}$$

For rotation in the other direction

$$\psi_{2,l} = -(2\pi l - \eta - \alpha) \ , \quad l = 1, 2, 3, \ldots \ . \tag{A11}$$

In order that $\psi_{1,0}$ not be negative, $\alpha \le \eta$ if $\eta < \pi/2$. For all other cases, $0 \le \alpha \le \pi/2$ since as $v_t \to 0$, $\alpha \to 0$, and as $v_t \to \infty$, $\alpha \to \pi/2$.

The differential probability P_T may be determined once the P_i's are found by integrating the probabilities of all the individual combinations of α, ψ, and $\mathbf{c}$ for which detection can occur over α. Thus,

$$P_T(\theta_L, \tilde{\theta}, \theta, \delta) = \left\{\int_{\alpha=0}^{\xi} P_1\, d\alpha + \int_{\alpha=0}^{\pi/2} P_2\, d\alpha\right\}(\sin\theta/\sin\eta)\, d\delta\, d\theta\, d\tilde{\theta} \ , \tag{A12}$$

where

$$\xi = \begin{cases} \eta & \text{if } \eta \le \pi/2 \\ \pi/2 & \text{if } \eta > \pi/2 \ , \end{cases} \tag{A13}$$

$1/\sin\eta$ is the ratio of infinitesimal solid angles at OA and OB, and $\sin\theta$ is the Jacobian for integration over θ. The P_i are given by

$$P_i = w(\theta,\phi)\, P_\alpha(\alpha)\, P_{\hat{c}}(\hat{c})\, J(\tilde{\theta})\, F(\hat{v})\, P_{i,\psi}(\eta - \alpha) \ , \tag{A14}$$

where $w(\theta,\phi)$ is given by Eq. (1), P_α is the probability of rotation angle α, $P_{\hat{c}}$ is the probability of the $\hat{c}$ determined using Eqs. (A4) and (A8), $J(\tilde{\theta}) = \cos\tilde{\theta}$ is the ratio of differential solid angle elements along the detector direction and OB,[5,7] and $F(\mathbf{v})$ is a correction due to detector flux sensitivity. For mass spectrometers, $F(\hat{v}) = 1/\hat{v}$ is determined from Eqs. (A4) and (A9), while for surface ionization detectors $F(\hat{v}) = 1$. $P_{1,\psi}$ is the probability of rotational angle $\psi_{1,0}$, while $P_{2,\psi}$ is the total probability of the rest of the $\psi_{i,l}$ defined in Eqs. (A10) and (A11), respectively. Note that since $\psi_{i,l}$ has an η dependence, η has a θ, δ, and γ dependence, and γ in turn has a $\tilde{\theta}$ and θ_L dependence, the $P_{i,\psi}$ are dependent on $\tilde{\theta}$, δ, θ, and θ_L, i.e., on the positions of OA, OB, and ϵ. The quantities used in Eq. (A14) are derived as follows. The expression for $P_{\hat{c}}(\hat{c})$ was derived previously[5] and is

$$P_{\hat{c}}(\hat{c})\, d\hat{c} = \hat{c}^2 \exp(-\hat{c}^2) d\hat{c} . \tag{A15}$$

The probability of a given angle α is derived[12] starting with the familiar Boltzmann distribution in rotational states

$$P_J(J)\, dJ = (2J+1)\exp(-J^2\hbar^2/2IkT)\, dJ \ , \tag{A16}$$

where J is the rotational quantum number, $\hbar$ is Planck's constant divided by 2π and I is the moment of inertia. In the limit of high rotational energies, which apply for heavy molecules,

$$I\omega = J\hbar \ , \tag{A17}$$

where ω is the angular velocity. The relation between the tangential velocity and angular velocity is

$$v_t = R\omega \ , \tag{A18}$$

where R is the equilibrium distance from the center of mass to the detected fragment in the parent molecule. In terms of the equilibrium bond length Eq. (A18) becomes

$$v_t = R_e\, \omega m_2/M \ , \tag{A19}$$

where m_2 is the mass of the undetected fragment. By appropriate substitution, where $J \gg 1$

$$P_x(x)\,dx = 2x \exp(-x^2)\,dx \ , \tag{A20}$$

where $x = v_t\, s$ and $s = [m_1 M/2m_2 kT]^{1/2}$. Since $v_t = u \sin\alpha$, from Eq. (A7) $x = v_t\, s = u_0 s \tan\alpha$. Thus the probability of a given α is related to the corresponding x:

$$P_\alpha(\alpha) = P_x(u_0 s \tan\alpha) \ . \tag{A21}$$

Combining Eq. (A19) with the preceding equations

$$\omega = x_a u_0 \tan\alpha \ , \tag{A22}$$

where $x_a = M/m_2 R_e$.

The excited state is assumed to have a Poisson distribution of lifetimes. In terms of angles this distribution is

$$f(\psi) = (1/\bar{\psi}) \exp(-\psi/\bar{\psi}) \ , \tag{A23}$$

where $\bar{\psi} = \tau\omega$ is the mean rotational angle corresponding to lifetime τ. Thus $\bar{\psi} = \tau x_a u_0 \tan\alpha$. Combining Eqs. (A10), (A11), and (A23)

$$P_{1,\psi} = (1/\bar{\psi}) \exp[(-\eta + \alpha)/\bar{\psi}] \ , \tag{A24}$$

$$P_{2,\psi} = (1/\bar{\psi}) \sum_{l=1}^{\infty} \{\exp[(-2\pi l - \eta + \alpha)/\bar{\psi}] + \exp[(-2\pi l + \eta + \alpha)/\bar{\psi}]\}$$

$$= (1/\bar{\psi}) \{\exp[(-2\pi - \eta + \alpha)/\bar{\psi}] + \exp[(-2\pi + \eta + \alpha)/\bar{\psi}]\}/$$

$$[1 - \exp(-2\pi/\bar{\psi})] \ . \tag{A24'}$$

The total probability P_D of recoil along arbitrary OB in the CM followed by detection in the LAB is found by integrating P_T over all positions of OA, that is, over all possible molecular positions. Thus

$$P_D(\mathrm{OB}, \theta_L)\,d\tilde{\theta} = 2\left[\int_0^{\pi}\int_0^{\pi} P_T\,d\delta\,d\theta\right] d\tilde{\theta} \ . \tag{A25}$$

Because of the symmetry of the distributions through the the plane, we have bounded the integration over δ by 0 and π instead of 0 and 2π and have included a factor of 2. The probability of detection at a given θ_L is found by integrating (A25) over the subset of all **u** directions which can lead to detection. Thus,

$$W(\theta_L) = \int_0^{\pi/2} P_D(\mathrm{OB}, \theta_L)\,d\tilde{\theta} \ . \tag{A26}$$

Equation (A26) then generates the LAB angular distribution which can be compared with experiment. Alternatively, the calculated curve can be fit to Eq. (3) and the values of B and θ_S compared with their experimental counterparts.

A copy of the ICM convolution program, listed in FORTRAN, is available to those who include with their request a specific statement outling the purpose for which the program will be used.

[1] R. S. Berry, in *Alkali Halide Vapors*, edited by P. Davidovits and D. L. McFadden (Academic, New York, 1979), p. 77.
[2] G. Herzberg, *Spectra of Diatomic Molecules* (Van Nostrand, Princeton, New Jersey, 1965).
[3] G. H. Busch, J. P. Cornelius, R. T. Mahoney, R. I. Morse, D. W. Schlosser, and K. R. Wilson, Rev. Sci. Instr. **41**, 1066 (1970).
[4] R. N. Zare, Mol. Photochem. **4**, 1 (1972).
[5] G. E. Busch and K. R. Wilson, J. Chem. Phys. **56**, 3626, 3638, 3655 (1972).
[6] S. Yang and R. Bersohn, J. Chem. Phys. **61**, 4400 (1974).
[7] W. R. Anderson, R. C. Ormerod and T. L. Rose, J. Chem. Phys. **62**, 127 (1975).
[8] W. R. Anderson, Ph. D. Dissertation, Texas A & M University (1977).
[9] R. C. Ormerod, T. R. Powers, and T. L. Rose, J. Chem. Phys. **60**, 5109 (1974).
[10] W. R. Anderson, B. M. Wilson, and T. L. Rose, Chem. Phys. Lett. **48**, 284 (1977).
[11] T. M. R. Su and S. J. Riley, J. Chem. Phys. **71**, 3194 (1979).
[12] R. C. Ormerod, Ph. D. Dissertation, Texas A & M University (1975).
[13] (a) T. R. Touw and J. W. Trischka, J. Appl. Phys. **34**, 3635 (1963). (b) K. R. Wilson and R. J. Ivanetich, University of California Radiation Laboratory Report, UCRL-11606 (1964).
[14] J. H. Ling and K. R. Wilson, J. Chem. Phys. **65**, 881 (1976).
[15] L. Brewer and E. Brackett, Chem. Rev. **61**, 425 (1961).
[16] W. Gordy, Pure Appl. Chem. **11**, 403 (1965).
[17] P. Davidovits and D. C. Brodhead, J. Chem. Phys. **46**, 2968 (1967).
[18] (a) C. Zener, Proc. R. Soc. A **137**, 696 (1932). (b) H. W. S. Massey, E. H. S. Burhop, and H. B. Gilbody, *Electronic and Ionic Impact Phenomena* (Oxford U. P., London, 1971), V. 2, p. 1915.
[19] D. Herschbach and R. Grice as tabulated in Ref. 32.
[20] G. M. Carter and D. Pritchard, J. Chem. Phys. **62**, 927 (1975).
[21] K. J. Kaufman, J. R. Lawter, and J. L. Kinsey, J. Chem. Phys. **60**, 4016 (1974).
[22] G. A. L. Delvigne and J. Los, Physica **67**, 166 (1973) and references therein.
[23] H. Levi, Doctoral Dissertation, Berlin (1934).
[24] M. Oppenheimer and R. S. Berry, J. Chem. Phys. **54**, 5058 (1971).
[25] R. S. Berry, J. Chem. Phys. **27**, 1288 (1957).
[26] R. A. Berg and G. W. Skewes, J. Chem. Phys. **51**, 5430 (1969).
[27] W. Koechner, *Solid State Laser Engineering* (Springer, New York, 1976), p. 51.
[28] M. A. D. Fluendy, D. S. Horne, K. P. Lawley and A. D. Morris, Mol. Phys. **19**, 659 (1970).
[29] W. Hack, F. Rosenkrantz, and H. G. Wagner, Z. Naturforsch. A **26**, 1128 (1971).
[30] K. J. Kaufman, J. L. Kinsey, H. B. Palmer, and A. Tewarson, J. Chem. Phys. **60**, 4023 (1974).
[31] J. J. Ewing, R. Milstein and R. S. Berry, J. Chem. Phys. **54**, 1752 (1971).
[32] P. Brumer and M. Karplus, J. Chem. Phys. **58**, 3903 (1973).
[33] L. W. Grossman, G. S. Hurst, M. G. Payne, and S. L. Allman, Chem. Phys. Lett. **50**, 70 (1977) and references therein.